

High proliferation rate and a compromised spindle assembly checkpoint confers sensitivity to the MPS1 inhibitor BOS172722 in triple negative breast cancers

Simon J Anderhub^{1§*}, Grace Wing-Yan Mak^{1*}, Mark D Gurden^{2§*}, Amir Faisal^{1§*}, Konstantinos Drosopoulos^{2*}, Katie Walsh^{1§}, Hannah L Woodward^{1§}, Paolo Innocenti^{1§}, Isaac M Westwood^{1§}, Sébastien Naud^{1§}, Angela Hayes¹, Efthymia Theofani^{1§}, Simone Filosto^{1§}, Harry Saville¹, Rosemary Burke¹, Rob LM van Montfort¹, Florence I Raynaud¹, Julian Blagg^{1§}, Swen Hoelder¹, Suzanne A Eccles^{1§} and Spiros Linardopoulos^{1,2}

¹Cancer Research UK Cancer Therapeutics Unit, Division of Cancer Therapeutics, The Institute of Cancer Research, London, United Kingdom;

²The Breast Cancer Toby Robins Research Centre, The Institute of Cancer Research, London, United Kingdom

[§]Current address: SA: s.anderhub@gmx.de; MDG: m.gurden@imperial.ac.uk; AF: Lahore University of Management Sciences, D.H.A. Lahore Cantt. 54792, Lahore, Pakistan, amir.faisal@lums.edu.pk; KW: Katie.walsh@pwc.com; HLW: hannah.woodward@ucl.ac.uk; PI: p.innocenti@biology.leidenuniv.nl; IMW: isaacmarkwestwood@gmail.com; SN: sebastien.naud@bayer.com; ET: efthymiatheofani@gmail.com; SF: simone.filosto@tusktherapeutics.com; JB: admin@neophore.com; SAE: Suzanne_e53@hotmail.com

* indicates equal contribution

Corresponding Authors: Spiros Linardopoulos, Team Leader, Cancer Research UK, Cancer Therapeutics Unit, The Institute of Cancer Research, 15 Cotswold Road, Sutton, SM2 5NG and Breast Cancer Now, 237, Fulham Road, London, SW3 6JB, UK. TEL: +44 20 7153 5341, EMAIL: spiros.linardopoulos@icr.ac.uk

Running title: MPS1 inhibitor BOS172722 in TNBC

Keywords: MPS1, Paclitaxel, Synergy, TNBC, Spindle Assembly Checkpoint

Abstract

BOS172722 (CCT289346) is a highly potent, selective and orally bioavailable inhibitor of spindle assembly checkpoint kinase MPS1. BOS172722 treatment alone induces significant sensitisation to death, particularly in highly proliferative triple negative breast cancer (TNBC) cell lines with compromised spindle assembly checkpoint activity. BOS172722 synergises with paclitaxel to induce gross chromosomal segregation defects caused by MPS1 inhibitor-mediated abrogation of the mitotic delay induced by paclitaxel treatment. In *in vivo* pharmacodynamic experiments, BOS172722 potently inhibits the spindle assembly checkpoint induced by paclitaxel in human tumour xenograft models of TNBC, as measured by inhibition of the phosphorylation of histone H3 and the phosphorylation of the MPS1 substrate, KNL1. This mechanistic synergy results in significant *in vivo* efficacy, with robust tumour regressions observed for the combination of BOS172722 and paclitaxel *versus* either agent alone in long-term efficacy studies in multiple human tumour xenograft TNBC models, including a patient-derived xenograft and a systemic metastasis model. The current target indication for BOS172722 is TNBC, based on their high sensitivity to MPS1 inhibition, the well-defined clinical patient population with high unmet need, and the synergy observed with paclitaxel.

Introduction

The key mechanism ensuring proper chromosome segregation during mitosis is the spindle assembly checkpoint (SAC), which monitors the correct bipolar attachment and tension of microtubules (MTs). When all microtubules have been properly attached to the kinetochores, the cells enter anaphase by releasing activators of the anaphase promoting complex/cyclosome (APC/C) (1,2). One of the pivotal proteins of the SAC is MPS1 kinase (also known as TTK). MPS1 is vital for the recruitment of kinetochore components, namely a complex of MAD2 and MAD1, to unattached kinetochores (3,4) which in turn bind and lock the APC/C co-activator cdc20, keeping the APC/C inhibitory complex inactive. MPS1 is further essential for sustaining this inhibitory complex throughout mitosis (5-7) and for correcting improperly attached chromosomes (8). Consequently, if MPS1 is inhibited, the time cells spend in mitosis is drastically reduced, resulting in elevated chromosome segregation errors and overall aneuploidy reaches detrimental levels (3,6,9,10). Whilst most cancers have a high frequency of aneuploidy (11,12) and chromosome instability (CIN) is a common feature (13-15), even these cells cannot tolerate aneuploidy beyond a certain threshold and increasing CIN has been shown to have a negative impact on their overall viability (16-18). Thus, instant generation of unsustainable aneuploidy induced by MPS1 inhibition poses an attractive area for therapeutic intervention in cancer and several inhibitors have been previously reported (19-26).

Breast cancer comprises distinct subtypes (27-29) with both human epidermal growth receptor 2 (HER2) overexpressing and basal-like breast cancer, including triple negative breast cancers (TNBC), having a significantly worse

prognosis than luminal and normal-like cancers (28,30-32). Within the distinct subgroups, TNBCs are associated with the highest proliferation rate and the expression of gene signatures associated with the cell cycle (29,33,34). For these reasons, antimitotic chemotherapy seems to be a rational option in TNBC and we sought to identify synergistic combinations with established therapeutics in order to maximize benefit while minimizing the potential for the emergence of secondary resistant tumours.

Material and Methods

Reagents and Antibodies

Eribulin was purchased from Eisai Pharmaceuticals, HOECHST33342 and DAPI from Life Technologies. All other reagents were obtained from Sigma.

Cell culture

Cell lines were purchased from ATCC and DSMZ. In-house authentication of cell lines by SNP profiling was carried out and cultured cells were passaged for less than 6 months before replacement from early passage frozen stocks. Cells were regularly screened for mycoplasma, using a PCR-based assay (VenorGem; Minerva Biolabs).

Cell based assays

We performed a High Throughput Screen at Horizon Discovery Inc. as described below. The endpoint readout of this assay is based upon quantitation of ATP as an indicator of viable cells (except when noted in Analyzer). Once cells reached expected doubling times, screening begins. Cells are equilibrated in assay plates via centrifugation and placed in CO₂ incubators (attached to the Dosing Modules) at 37°C for twenty-four hours before treatment. At the time of treatment, a set of assay plates (which do not

receive treatment) are collected and ATP levels are measured by adding ATPLite (Perkin Elmer). These T-zero (T0) plates are read using ultra-sensitive luminescence on Envision plate readers. Assay plates are incubated with compound (10-point treatment) for 120 hours and are then analysed using ATPLite. All data points are collected via automated processes and are subject to quality control. GI_{50} and Synergy was determined using Horizon's proprietary software, Chalice. Assay plates are accepted if they pass the following quality control standards: relative raw values are consistent throughout the entire experiment, Z-factor scores are greater than 0.6 and untreated/vehicle controls behave consistently on the plate. GI_{50} determination in Breast Cancer cell lines was carried out in-house in 384 (Greiner Bio-One, #781091), as described below. Cells were seeded at individual optimal cell densities and drugs added using an Echo liquid handler (Labcyte). After 5 days cells were incubated with HOECHST 33342 stain (10 μ g/ml) and Propidium iodide (1 μ g/ml) and assays read on a Celigo Imaging Cytometer (Nexcelom) using the Dead&Total application. GI_{50} s were assessed using GraphPad prism and a sigmoidal fit. For synergy screening in breast cancer cell lines, the respective drug concentrations were: 0.001 and 0.002 μ M Paclitaxel, 0.0001 and 0.0002 μ M eribulin, 0.002 and 0.004 μ M doxorubicin and analysis was performed using the "Macsynergy™II" spreadsheet. In brief, cells were seeded at optimal densities in 96 well plates. BOS172722 and Paclitaxel were added at a fixed ratio determined by the respective GI_{50} s for each compound and cell line. Cell viability was assayed after 5 days using the MTT reagent and calculations were done using the Compusyn program.

Meso Scale Discovery (MSD) assay

In-house electrochemiluminescence (Meso Scale Discovery, MSD) assays were developed to measure tubulin acetylation and histone H3 phosphorylation. After treatment, cells were washed with PBS and lysed with RIPA buffer (150mM NaCl, 50mM Tris pH 7.5, 1mM EDTA pH 8.0, 1% (v/v) NP40, 1% sodium deoxycholate, 0.1% SDS, 10mM NaF, protease inhibitor tablet, and phosphatase inhibitor cocktails) and sonicate briefly (3-4 pulses at mid power). Protein lysates were then diluted 1:10 in lysis buffer (50mM NaCl, 20mM Tris pH 7.5, 1mM EDTA, 1mM EGTA, 1% (v/v) Triton X-100, 10mM NaF, protease inhibitor tablet and phosphatase inhibitor cocktails) to be compatible with the MSD buffer content required. For the acetylated tubulin MSD assay, 25µL of lysate (0.2-0.4µg/µl) was loaded onto MSD plates that were pre-coated with anti-tubulin antibody (1:100 in PBS, mouse monoclonal, Sigma, cat. no. 9026) and blocked with 3% (w/v) BSA, and protein lysates were incubated on the plate for 1h at room temperature on a shaker. Plates were washed with MSD wash buffer, and 25µL of anti-acetylated tubulin Antibody (rabbit polyclonal, Cell Signaling, cat. no. 5335) 1:100 diluted in 1% (w/v) BSA was added followed by incubation for a further 1h at RT. Plates were washed with MSD wash buffer and incubated with 25µL of anti-rabbit sulfo-TAG antibody (Meso Scale Discovery, cat. no. R32AB) diluted in 1% (w/v) BSA) for 1h. After the final incubation, plates were washed with MSD wash buffer and read in the presence of 1xMSD read buffer. IC₅₀ values were determined using GraphPad PRISM. For phosphorylated histone H3 MSD assay, the same preparation was used except that the plate was pre-coated with anti-

pan histone antibody (2µg/ml diluted in PBS, mouse monoclonal, Millipore, cat. no. MAB3422) and anti-phospho histone H3 antibody (rabbit polyclonal, Millipore, cat. no. 06-570) 1:100 diluted in 1% (w/v) BSA was used to detect the phosphorylated Histone H3.

Flow cytometry

Flow cytometry to determine the cell cycle profile in HeLa cells after treatment with 100nM and 200nM BOS172722 for 24h, was performed as previously described (23).

Metaphase spreads

Cells were seeded in 10 cm dishes. The next day, Paclitaxel or 0.25% DMSO was added. After 36h, cells were arrested using nocodazole (100ng/ml) and further incubated for 4 hours. Mitotic cells were collected via mitotic shake off, pelleted, re-suspended in 0.75mM KCl and incubated at 37°C for 8 minutes. After centrifugation, cells were fixed using a -20°C solution of 4:1 methanol:acetic acid. Cells were pelleted and fixative removed. 15µl of cell suspension was dropped onto a glass slide and stained with 10µg/ml DAPI. Pictures were taken on a Zeiss Imager.D1 microscope equipped with an AxioCam MRm using Axiovision software (Zeiss).

Live cell imaging, immunofluorescence and immunoprecipitation

Analysis by immunofluorescence and time lapse microscopy as well as immunoprecipitations were performed as previously described (7).

Immunohistochemistry and immunofluorescence in human tumour xenografts

Tumours were fixed in 10% neutral buffered formalin and embedded in paraffin. Phosphorylation of T875 on KNL1 was determined by

immunohistochemistry. Heat-based antigen retrieval was performed by boiling the 4-mm-thick tissue sections in pH=6 citrate buffer (TCS Biosciences Ltd., HDS05, 1:100 dilution) for 5 min in a pressure cooker. The sections were incubated with a rabbit polyclonal T875-KNL1 antibody for 2h and detected using a Vectastain Elite ABC kit (Vector Laboratories) and DAB reagent (Dako). Nuclei of the cells were located by counterstaining the sections with Harris' haematoxylin. The T875-KNL1 antibody was generated by immunizing rabbits with phosphorylated peptides CNDMDI(pT)KSYTI (Eurogentec). T875-KNL1 positive cells were quantified by manually counting positively stained cells in 8 random fields of the tumour section. Phosphorylation of Histone H3 was determined by immunofluorescence. Heat-based antigen retrieval was performed as described above, except that the slides were heated in the microwave for 10 min. The sections were incubated with rabbit polyclonal p-histone H3 (S10) antibody (Millipore, 06-570) for 1h, then incubated with secondary goat anti-rabbit IgG (H+L) Alexa Fluor 488 (Invitrogen, A-11034) and counterstained with DAPI. For each section, 9 fluorescent images were captured and quantification of p-Histone H3 positive cells was done in CellProfiler software (www.cellprofiler.org).

Real-Time quantitative PCR

RNA from cells was extracted using the Quick-RNA™ kit (Zymo Research) according to the manufacturer's instructions. Real-time quantitative PCR reactions of the MPS1 gene were carried out using the TaqMan Universal PCR Master Mix (Applied Biosystems) in the Applied Biosystems StepOne-plus Real-time PCR System, following the manufacturer's instructions. We used commercially available primers and probes for PCR analyses (TaqMan

Gene Expression Assays, Assay ID: Hs01009870_m1 for MPS1, and Hs03003631_g1 for 18S and Hs04195421_s1 for PP1A as endogenous controls; Applied Biosystems). PCR conditions were as follows: 95°C for 10 min, followed by 40 cycles at 95°C for 15 sec and 60°C for 1 min. Each sample was assayed in triplicate with RNase-free water as negative control. Relative gene expression quantifications were calculated according to the comparative Ct method using 18S or PP1A as an endogenous control. Final results were determined by the formula $2^{-\Delta\Delta Ct}$.

In vivo efficacy studies

The MDA-MB-468 and the OD-BRE-503 patient-derived xenograft studies were carried out at Oncodesign S.A., France. Statistical analyses of mean tumour volumes at randomisation were performed using ANOVA and pairwise tests were performed using the Bonferroni/Dunn correction in case of significant ANOVA results. A p -value < 0.05 was considered as significant. For the metastatic model, MDA-MB-231 luciferase-expressing cells were injected iv in the tails of NOD SCID mice. Mice were dosed starting 6 days after tumour cell implantation, with Paclitaxel at 15mg/kg on days 0 (day 0 is 6th day after tumour cell implantation), 7, 14 and 21 i.v. and BOS172722 at 30 and 40mg/kg p.o. on days 0+1, 7+8, 14+15 and 21+22 and tumour burden was assessed by whole body bioluminescent imaging (BLI). Animals were culled when they showed signs of deterioration due to tumour burden (body weight loss, rapid breathing). All animal studies were carried out in accordance with the UK Animals (Scientific Procedures) Act 1986 and national guidelines (35).

Results

BOS172722 is a novel, potent and orally bioavailable MPS1 inhibitor in biochemical and cellular assays

BOS172722 is a novel, orally bioavailable, potent and highly selective small molecule inhibitor of MPS1 kinase discovered from our in-house lead optimization studies on a pyridopyrimidine series of compounds (Figure 1A; (36)). *In vitro* kinase assays using purified recombinant MPS1 protein showed that BOS172722 inhibited MPS1 activity with IC_{50} values of 0.004 μ M at low ATP (10 μ M) and 0.01 μ M, at high (1mM) ATP concentrations respectively (Figure 1A). The *in vitro* profiling of BOS172722 was tested in a wide panel of more than 400 kinases (36). Only a small number of other kinases were inhibited by BOS172722, in particular JNK1, JNK2, JNK3 and LRRK2 at >80% at 1 μ M. Follow up IC_{50} values were obtained (JNK1 IC_{50} = 0.092 μ M, JNK2 IC_{50} = 0.076 μ M, JNK3 IC_{50} = 0.242 μ M and LRRK2 IC_{50} = 0.048 μ M) showing that BOS172722 is highly selective for MPS1 over these other kinases (36). We have previously described the use of an in-house electrochemiluminescence (Meso Scale Discovery, MSD) assay to quantitatively measure MPS1 auto-phosphorylation in cells at T33/S37 sites (22,23). BOS172722 potently inhibited MPS1 T33/S37 auto-phosphorylation in MSD assay with IC_{50} value of 0.06 ± 0.03 μ M (Figure 1A). To prove that the observed inhibition of MPS1 phosphorylation it is not a consequence of a mitotic exit, nocodazole-arrested HCT116 cells, a colon cancer cell line sensitive to MPS1 inhibition widely used for MPS1 activity investigation (20),

were co-treated with BOS172722 and MG132 proteasome inhibitor to block exit from mitosis, for 2h. Nocodazole-induced MPS1 auto-phosphorylation on T33/S37 was completely inhibited by treatment with BOS172722, indicating that BOS172722 specifically inhibits the activity of MPS1 (Figure 1B). Next, HCT116 cells treated with different concentrations of BOS172722 for 24 and 48h were analysed for inhibition of histone H3 phosphorylation and PARP cleavage by immunoblotting. Histone H3 phosphorylation at Ser10 was inhibited in a time-dependent manner (Supplementary Figure S1A). Induction of apoptotic cell death upon drug treatment also increased as determined by levels of cleaved PARP (Supplementary Figure S1A). To identify the time that is required for BOS172722 to induce maximum effect on tumour cell growth inhibition, we performed wash-off experiments. HCT116 cells were treated with BOS172722 for 2 to 96h followed by the measurement of growth inhibition (GI_{50} s) at 96h. We observed that 24h of treatment showed a comparable GI_{50} to 96h treatment (Supplementary Figure S1B), indicating that 24h of MPS1 inhibition is sufficient to achieve maximum growth inhibition in tumour cells.

Effects of BOS172722 on spindle assembly checkpoint activity and cell cycle

MPS1 activity is required for activation of SAC and inhibition of its activity results in SAC override and mis-segregation of chromosomes. In order to investigate the mechanism of action of BOS172722, we performed live cell imaging of H2B-mCherry-transfected HeLa cells, a model widely used to study mitosis. We measured time in mitosis and chromosome segregation

defects after treatment with BOS172722. We found that treatment with 200nM of BOS172722 resulted in early mitotic exit of 11 minutes compared with 52 minutes for the untreated HeLa cells (Figure 1C). This sharp decrease in time in mitosis resulted in gross chromosomal abnormalities including unaligned chromosomes (~83%) and decondensation of chromosomes without division (~17%; Figures 1D). In addition, induction of aneuploidy and loss of normal cell cycle profile was observed in cells treated with BOS172722 for 24 hrs with the indicated concentrations (Figure 1E). MPS1 activity is required for the recruitment of SAC components to the unattached kinetochores. To test this, HeLa cells were pre-treated with BOS172722 for 1 hour, then treated with nocodazole, MG132 and BOS172722 for an additional 1 hour to arrest the majority of cells in mitosis, followed by fixation and staining with the indicated antibodies (Supplementary Figure S1C). Treatment of cells with 200nM BOS172722 resulted in loss of recruitment of MAD1, MAD2, BUBR1, and KNL1 to the unattached kinetochores. A reduction in MPS1 T33/S37 auto-phosphorylation was also observed with BOS172722 treatment, whereas MPS1 levels at kinetochores remained unchanged (Supplementary Figure S1C).

Cell proliferation rate and SAC activity are important indicators for BOS172722 potency

Prompted by the observation that PTEN-deficient cell lines are more sensitive to MPS1 inhibition (37) and in order to identify additional populations that may benefit from an MPS1 inhibitor, we tested 50 cancer cell lines, including 25

PTEN-proficient and 25 PTEN-deficient, with BOS172722 in a 5-day growth inhibition assay (Supplementary Table S1A). The results showed that, although there is a clear trend in sensitivity to MPS1 inhibition with BOS172722 between PTEN-deficient and PTEN-proficient cell lines, the difference was not statistically significant (Figure 2A). Treatment of 50 cancer cell lines from 8 different tissues of origin, in addition to the data we have generated using TNBC cell lines, showed that lung cancer cell lines overall show similarly sensitivity to MPS1 inhibition (Supplementary Figure S2A). In addition, similar to TNBC cell lines, the average doubling time of the cell lines above the median GI_{50} was higher than the average doubling time of the cell lines below the median GI_{50} . Moreover, there was a statistically significant difference between the doubling time of the most sensitive cell lines (top tercile, $n=17$, 38 hrs) relative to the rest of the cell lines ($n=33$, 53 hrs; Figure 2B), suggesting that more rapidly dividing cells show greater susceptibility to MPS1 inhibition. Towards the identification of mutations that could predict sensitivity to BOS172722, we extracted non-silent mutations in the coding regions of genes for 16 sensitive cell lines ($GI_{50} < 50nM$) and 16 resistant cell lines ($GI_{50} > 200nM$) from the Cancer Cell Line Encyclopaedia (CCLE) database and looked for enrichment of mutated genes in the sensitive group. We selected genes that were mutated in at least 3 cell lines in the sensitive group over the resistant group and in no more than two cell lines in the resistant group and calculated the fold enrichment in the two sets (Supplementary Table S1B). The most enriched mutated gene in the sensitive group was PI4KB, a protein that has been shown to be active in mitosis (38) and to prevent formation of polylobed nuclei (39) which is indicative of mitotic

exit with aberrant chromosome segregation and aneuploidy (Figure 2C). Similarly, mutations in ARID1A and SMARCA4 have been shown to induce genomic instability and aneuploidy (40) that is further increased to intolerable levels by MPS1 inhibition, resulting in cell death. In addition, mutations in NUMA1 and TPR, that have been shown to be involved in mitotic spindle assembly and in the activation of the SAC (41-43), may directly sensitise cells to MPS1 inhibition.

We have previously shown that basal breast cancer cell lines (including TNBC) were more sensitive to our tool compound MPS1 inhibitor CCT271850 in comparison to luminal breast cancer cell lines (23). To investigate further, we used a panel of TNBC and non-TNBC cell lines to investigate the association between the potency of BOS172722 to: a) TNBC *versus* non-TNBC cell lines; b) MPS1 expression; c) proliferation rate and d) SAC activity. We confirmed that TNBC cell lines are more sensitive to BOS172722 in comparison with non-TNBC cell lines (Supplementary Figure S2B and Supplementary Table S2). Our data from breast cancer cell lines are in agreement to the published data from primary breast tumours (44) that MPS1 expression is higher in TNBC *versus* non-TNBC cell lines (Supplementary Figures S2C,D). Importantly, we found that the cellular potency of BOS172722 at Emax (representing maximum effect) significantly associated with the proliferation rate of the cell lines as measured by their doubling times (Figure 2D), similar to the panel of the 50 cell lines from different types of human cancers described above (Figure 2B); TNBC cell lines, being more sensitive, have shorter doubling times (Supplementary Figure S2E). We then investigated the association between BOS172722 potency and levels of SAC

activity. To our surprise, cell lines with reduced SAC activity, as measured by MPS1 phosphorylation and BUB1 localisation upon mitotic arrest, were more sensitive to BOS172722 treatment (Figures 2E,F, Supplementary Table S2), indicating that cell lines with a compromised SAC may require lower doses of an MPS1 inhibitor to abrogate the mitotic checkpoint, thereby inducing gross chromosomal abnormalities and cell death. TNBC cell lines overall showed an overall weaker SAC. A t-test or a one-way ANOVA, shows p -value <0.009 . However, we used the u-test as these data failed to pass the Shapiro-Wilk normality test. Based on u-test, TNBC cells have on average lower pMPS1/mitotic index ratios (mean 4.75, standard deviation 2.31) relative to non-TNBC cells (mean 32.5, standard deviation 21.6), including two extreme non-TNBC outliers with ratios of 1.1 and 2.2. However, although low ratios may be found in other populations, TNBC cells represent a homogenous group. These data together suggest that the proliferation rate together with the SAC activity may potentially be used as stratification markers for TNBC patient selection to achieve maximum efficacy.

BOS172722 shows synergistic effect with paclitaxel in TNBC cell lines

Based on its promising *in vitro* profile, we progressed BOS172722, to human tumour xenograft models of TNBC to initially evaluate single agent efficacy. In established orthotopic MDA-MB-231 xenografts, BOS172722 given at 50mg/kg orally, twice a week for 47 days showed significant but moderate reduction of tumour growth compared with vehicle-treated mice (tumour growth inhibition: TGI = 66%, $p = 0.0001$; Supplementary Figure S3).

However, to support clinical trials as a single agent would require evidence of tumour stasis or regression in preclinical models. We therefore screened a panel of TNBC cell lines for synergism between BOS172722 with paclitaxel (Tax) at 1 and 2nM, doxorubicin (Dox) at 2 and 4nM and eribulin (Eri) at 0.1 and 0.2nM, to a wide range of BOS172722 concentrations (0 to 500nM). The data were then analysed using MacSynergyII (45). Of the combinations of compounds tested, only paclitaxel with BOS172722 showed consistent synergy across our panel of TNBC cell lines (Figure 3A). By contrast, treatment of BOS172722 together with eribulin or doxorubicin did not show any synergy in the majority of the cell lines tested, with few exceptions (Figure 3A). We therefore focused on further characterising the mechanism of the synergism between BOS172722 and paclitaxel. In our screen, we used concentrations of 1 and 2nM of paclitaxel and the maximum synergism was observed at 1nM or <2nM for all cell lines (Supplementary Table S3). Importantly, the observed synergistic concentrations were relevant to the clinical concentrations of paclitaxel (46). In addition, the paclitaxel concentrations where maximum synergy is observed are either at or below the respective GI₅₀s of paclitaxel alone and are related to clinical dosing schedules (46) (Supplementary Table S3).

In order to investigate the mechanism of action of the synergism of paclitaxel with BOS172722, we performed flow cytometry analysis of the cell cycle of MDA-MB-231 after treatment with each drug individually or in combination. Treatment of MDA-MB-231 cells with 1nM paclitaxel or 100nM BOS172722 for 24h did not show any significant cell cycle effect on the cells. However, the

combination of both agents led to a pronounced decrease in height and broadening of the G1 cell cycle peak, consistent with the induction of aneuploidy (Figure 3B). At these drug concentrations the cell cycle profile was completely abolished (an expected minor effect on the cell cycle histogram was observed at 2nM paclitaxel alone; Figure 3B).

MPS1 inhibition reduces paclitaxel-induced mitotic delay and potentiates gross chromosome mis-segregation errors

The therapeutic effect of paclitaxel had long been attributed to the induction of a mitotic arrest (activating the SAC), resulting in cell death. Recent work however, demonstrated that paclitaxel exerts its effect mainly by the induction of aneuploidy via a multipolar mitosis (46). In contrast, MPS1 inhibition leads to premature abrogation of the SAC and as a consequence, detrimental aneuploidy (7).

We first assessed the abrogation of mitotic checkpoint by each drug, both individually and in combination using live cell microscopy of HeLa cells. Incubation of cells with BOS172722 resulted in a dose-dependent decrease in the median length of time cells spent in mitosis (Figure 3C). In order to measure the type and the magnitude of the chromosomal damage induced by combining BOS172722 and paclitaxel, we performed live cell imaging of H2B-mCherry transfected HeLa cells. We could thereby quantify chromosome segregation errors induced by the single agents and their combinations. As seen in Figure 3D, paclitaxel or BOS172722 at low concentrations alone

induce minor mitotic abnormalities. At higher concentrations of the individual drugs, the drug inherent phenotypes were evident: paclitaxel induces mainly multipolar mitotic figures in contrast to BOS172722, which predominantly induced division with unaligned chromosomes. In the case of the combination of both drugs, the number of abnormal mitosis which mainly exhibit unaligned chromosomes is synergistically increased. Importantly, even at 1nM concentration of paclitaxel, where the highest synergy scores were observed in our screen of growth inhibition, it induces only low levels of aneuploidy. We confirmed this result in MDA-MB-231 cells using metaphase spreads (Supplementary Figure S4A). Since both MPS1 inhibition and paclitaxel treatment cause chromosome alignment errors, we reasoned that the synergy between paclitaxel and BOS172722 may arise through increasing the amount of erroneous MT-kinetochore attachments. Indeed, using immunofluorescence-based assays, the amount of chromosome alignment errors increased following combination of the drugs, only additively, in all tested combinations, when mitotic exit was prevented with MG132 (Supplementary Figure S4B,C).

Paclitaxel induces a weak mitotic checkpoint delay

Because we did not observe consistent synergy with eribulin in our initial screen, we then investigated whether a SAC which has been activated to the same extent by MT-depolymerizing or whether MT-stabilizing drugs shows a differential response to MPS1 inhibition. In order to achieve comparable checkpoint activation with microtubule depolymerizing and stabilizing agents, we treated HeLa cells with nocodazole or paclitaxel and determined the

concentration at which maximal activation of the checkpoint was achieved as observed by a plateau in mitotic timing. Cells were then arrested for 16h with the respective MT poisons, different doses of BOS172722 added and the fraction of cells in mitosis measured. Of note, treatment with the respective concentrations of nocodazole or paclitaxel alone led to a very similar duration of the time cells remained arrested in mitosis (Figure 4A). In both cases, the mitotic block was overcome by MPS1 inhibition but, markedly, in paclitaxel arrested cells, this override was achieved with much lower concentrations of BOS172722 compared with nocodazole. A comparable rate of mitotic exit was achieved with 25nM BOS172722 in paclitaxel-arrested cells and 100nM BOS172722 (4 times the concentration) in nocodazole-arrested cells. We therefore considered that the maximal SAC induced by microtubule depolymerizing agents is comparably stronger than the analogous SAC induced by paclitaxel. In line with this hypothesis, when we analysed the recruitment of BUB1 to the kinetochore by immunofluorescence, BUB1 levels were, on average markedly lower in the cells arrested with paclitaxel, being on average 50% of the levels seen in nocodazole and with a much larger range (Figure 4B). Taken together, these data, suggest that the override of the weak paclitaxel-induced SAC with low concentrations of BOS172722 may explain the synergistic increase in cell death.

Simultaneous combination of BOS172722 with paclitaxel for 24h induces maximum synergy

In order to better delineate the time that is required for the combination of paclitaxel and BOS172722 to exert a synergistic effect, we incubated MDA-

MB-231 cells with BOS172722 for distinct periods of time and analysed the induced synergism with paclitaxel. We observed that incubation of both drugs for 12h had only a limited synergistic effect in MDA-MB-231 cells (Supplementary Figure S4D). We then explored the synergy of paclitaxel and BOS172722 in association with the incubation time in wash-off long-term clonogenic assays in MDA-MB-231 cells. We found that the combination of 1nM paclitaxel with 10nM BOS172722 was as efficacious as higher concentrations of each individual drug (Figure 4C). We were also interested in investigating whether sequential addition of the drugs had any benefit over simultaneous treatment on the degree of synergism seen. The addition of BOS172722 following paclitaxel treatment or the opposite, had no superior effect over the simultaneous addition (Supplementary Figure S4E). Therefore, simultaneous administration of drugs is potentially the most beneficial in clinical studies. Based on our data we propose the following model (Figure 4D): treatment with Paclitaxel induces mitotic arrest with unaligned chromosomes due to impaired microtubule dynamics and partial inactivation of the SAC due to the presence of kinetochore-microtubule attachments in some chromosomes. Cancer cells can escape mitotic arrest by mitotic slippage and/or following metabolism/excretion of the drug. Not all cells will have lethal levels of chromosomal abnormalities. Treatment with Paclitaxel in combination with BOS172722 completely prevents chromosome alignment in cancer cells due to impaired microtubule dynamics and dramatically reduced time in mitosis. All cells exit mitosis with gross chromosomal abnormalities and are not viable.

***In vivo* pharmacodynamic activity of BOS172722**

In pharmacodynamic (PD) experiments *in vivo* BOS172722 potently inhibits the SAC induced by paclitaxel in human tumour xenograft models of TNBC (MDA-MB-231), as measured by inhibition of the mitotic marker phosphorylated histone H3 (p-HH3) by immunofluorescence microscopy (Figure 5A right graph and 5B lower panel). We confirmed that this effect is mediated by MPS1 inhibition by demonstrating reduction of the mechanism-related proximal biomarker phosphorylated-KNL1 (p-KNL1) by immunohistochemistry (IHC; Figure 5A left graph and 5B upper panel). KNL1 is a natural substrate of MPS1 and is phosphorylated upon initiation of SAC activation by MPS1 (47).

Having shown that BOS172722 abrogates SAC as measured by paclitaxel-induced p-HH3 and p-KNL1 inhibition, we investigated whether we could identify target-engagement biomarkers to measure the activity of both paclitaxel and BOS172722 simultaneously in the same samples. It is known that taxanes induce acetylation of tubulin due to tubulin polymerisation (48), when at the same time MPS1 inhibition should not affect tubulin modification. Paclitaxel and BOS172722 was administrated simultaneously into HCT116 tumour bearing mice. Figure 5C shows paclitaxel-induced acetylation of tubulin at all time points while addition of BOS172722 had no effect on tubulin acetylation. In contrast, paclitaxel-induced histone H3 phosphorylation was significantly inhibited by BOS172722 at 2 and 6h. To optimise these assays in a high throughput format, we developed quantitative electrochemiluminescence assays (MSD). The results confirmed the

immunoblotting data, indicating a potential use of these biomarkers in the clinic (Figure 5D).

Therapeutic activity of BOS172722 in *in vivo* TNBC models

Based on *in vitro* activity and PD data, human TNBC xenograft experiments in athymic mice were undertaken to evaluate the therapeutic activity of paclitaxel alone or in combination with BOS172722. We initially used an MDA-MB-468 orthotopic (mouse mammary fat pad) xenograft model. Combination of BOS172722 with paclitaxel gave significant tumour regressions and a clear benefit in comparison with paclitaxel alone (Figure 6A). A study using a TNBC patient-derived xenograft (PDX) model also showed tumour regression and a significant benefit of combination treatment in comparison with paclitaxel alone (Figure 6B).

We then performed *in vivo* studies using a TNBC model to simulate breast cancer metastases. Tail-vein-injected MDA-MB-231-luciferase-expressing TNBC cells in SCID mice give rise predominantly to lung metastases. On day 28, the flux expressed as % of vehicle control was as follows: paclitaxel alone 18.8%; combination with BOS172722 at 30mg/kg 4.8% and 40mg/kg 5.7% confirming a significant benefit of combination treatment in both tumour growth and survival (up to day 63) at BOS172722 doses \geq 30mg/kg (Figure 6C,D). Taken together, the data described above demonstrate that our selective MPS1 inhibitor BOS172722 in combination with paclitaxel synergistically induces increased cell death in TNBC cell lines *in vitro* and

regression and/or reduced growth rate of human tumour xenografts *in vivo* compared to treatment with either agent alone.

Discussion

We initially discovered MPS1 as a potential therapeutic target during a siRNA screening campaign where we showed that a subgroup of breast cancer cell lines with a deregulated PTEN tumour suppressor gene were susceptible to cell death upon MPS1 depletion (37). We further investigated these findings using BOS172722. Fifty cell lines, 25 PTEN-proficient and 25 PTEN-deficient from a variety of human cancer types were tested upon treatment with BOS172722. We found a clear trend of sensitivity to BOS172722 of cell lines with PTEN deficiency, irrespective of the type of cancer. Although not statistically significant, patients with PTEN deficient tumours may represent a target population for treatment with an MPS1 inhibitor. However, the strongest, statistically significant corollary of sensitivity to MPS1 inhibition was cell proliferation rate. Cells with shorter doubling times were more sensitive to death upon MPS1 inhibition, TNBC cell lines being the most sensitive. A novel indicator for sensitivity to MPS1 inhibition is the SAC activity. We found that cell lines with reduced SAC activity were more sensitive to BOS172722, suggesting that lower SAC activity requires reduced concentrations of the MPS1 inhibitor to abrogate mitosis, thus inducing detrimental aneuploidy in cancer cells.

Due to the moderate levels of tumour growth inhibition by BOS172722 in xenograft studies, we focused on combination studies with the standard-of-

care agents in TNBC. We identified paclitaxel as a favourable combination agent for use with MPS1 inhibition as it exerts robust synergistic effects throughout our panel of TNBC cell lines. This combination has also been identified by others and clinical trials have been initialized (19,49; NCT02366949). Importantly, we discovered that a reduced SAC checkpoint is easier to override with an MPS1 inhibitor.

The same MPS1 mechanism of action is observed in paclitaxel-treated human TNBC xenografts *in vivo*. Athymic mice carrying TNBC human tumour xenografts were treated with vehicle, paclitaxel alone at clinically relevant dose or in combination with single dose BOS172722. Immunofluorescence microscopy and immunohistochemistry of tumour sections showed a significant reduction of phospho-histone H3 and reduction of phospho-KNL1. These data confirm the mechanistic contribution of MPS1 inhibition *in vivo*. In addition, we have suggested a novel target engagement biomarker strategy to be able to measure simultaneously the effect of paclitaxel and BOS172722 in tumour biopsies. The therapeutic benefit of BOS172722 in combination with paclitaxel was demonstrated in three TNBC *in vivo* models: MDA-MB-468 orthotopically transplanted in mouse mammary fat pads, systemic metastatic MDA-MB-231 and in a TNBC patient derived xenograft.

In summary, BOS172722 is a highly potent and selective, orally bioavailable MPS1 inhibitor with favourable PK. Robust efficacy was demonstrated at well tolerated doses in combination with paclitaxel in multiple xenograft models of TNBC, including PDX. BOS172722 is now in Phase I dose escalation clinical

trials in combination with standard of care paclitaxel treatment (NCT03328494).

Disclosure of Potential Conflicts of Interest

All authors are employees of The Institute of Cancer Research which has a commercial interest in drug development programs (see www.icr.ac.uk). Please note that all authors who are, or have been, employed by The Institute of Cancer Research are subject to a 'Rewards to Inventors Scheme' which may reward contributors to a programme that is subsequently licensed.

Acknowledgements and Grand Support

This work was supported by Cancer Research UK [grant number C309/A11566]. We also acknowledge the Cancer Research Technology Pioneer Fund and Sixth Element Capital for funding and NHS funding to the NIHR Biomedical Research Centre. SL, MDG and KD are also supported by Breast Cancer Now [grant ref: CTR-Q3].

References

1. Foley EA, Kapoor TM. Microtubule attachment and spindle assembly checkpoint signalling at the kinetochore. *Nature reviews* **2013**;14:25-37
2. Lara-Gonzalez P, Westhorpe FG, Taylor SS. The spindle assembly checkpoint. *Curr Biol* **2012**;22:R966-80
3. Sliedrecht T, Zhang C, Shokat KM, Kops GJ. Chemical genetic inhibition of Mps1 in stable human cell lines reveals novel aspects of Mps1 function in mitosis. *PLoS One* **2010**;5:e10251
4. Tighe A, Staples O, Taylor S. Mps1 kinase activity restrains anaphase during an unperturbed mitosis and targets Mad2 to kinetochores. *J Cell Biol* **2008**;181:893-901
5. Maciejowski J, George KA, Terret ME, Zhang C, Shokat KM, Jallepalli PV. Mps1 directs the assembly of Cdc20 inhibitory complexes during interphase and mitosis to control M phase timing and spindle checkpoint signaling. *J Cell Biol* **2010**;190:89-100

6. Hewitt L, Tighe A, Santaguida S, White AM, Jones CD, Musacchio A, *et al.* Sustained Mps1 activity is required in mitosis to recruit O-Mad2 to the Mad1-C-Mad2 core complex. *J Cell Biol* **2010**;190:25-34
7. Gurden MD AS, Faisal A & Linardopoulos S. Aurora B prevents premature stripping of spindle assembly checkpoint proteins from the kinetochore: a novel role for Aurora B in mitosis. *Oncotarget* **2016**; 28:19525-42
8. Santaguida S, Tighe A, D'Alise AM, Taylor SS, Musacchio A. Dissecting the role of MPS1 in chromosome biorientation and the spindle checkpoint through the small molecule inhibitor reversine. *J Cell Biol* **2010**;190:73-87
9. Kwiatkowski N, Jelluma N, Filippakopoulos P, Soundararajan M, Manak MS, Kwon M, *et al.* Small-molecule kinase inhibitors provide insight into Mps1 cell cycle function. *Nat Chem Biol* **2010**;6:359-68
10. Daniel J, Coulter J, Woo JH, Wilsbach K, Gabrielson E. High levels of the Mps1 checkpoint protein are protective of aneuploidy in breast cancer cells. *Proc Natl Acad Sci U S A* **2011**;108:5384-9
11. Duijf PH, Schultz N, Benezra R. Cancer cells preferentially lose small chromosomes. *International journal of cancer* **2013**;132:2316-26
12. Weaver BA, Silk AD, Montagna C, Verdier-Pinard P, Cleveland DW. Aneuploidy acts both oncogenically and as a tumor suppressor. *Cancer cell* **2007**;11:25-36
13. Heilig CE, Loffler H, Mahlknecht U, Janssen JW, Ho AD, Jauch A, *et al.* Chromosomal instability correlates with poor outcome in patients with myelodysplastic syndromes irrespectively of the cytogenetic risk group. *Journal of cellular and molecular medicine* **2010**;14:895-902
14. Lengauer C, Kinzler KW, Vogelstein B. Genetic instability in colorectal cancers. *Nature* **1997**;386:623-7
15. Yoon DS, Wersto RP, Zhou W, Chrest FJ, Garrett ES, Kwon TK, *et al.* Variable levels of chromosomal instability and mitotic spindle checkpoint defects in breast cancer. *The American journal of pathology* **2002**;161:391-7
16. Kops GJ, Foltz DR, Cleveland DW. Lethality to human cancer cells through massive chromosome loss by inhibition of the mitotic checkpoint. *Proceedings of the National Academy of Sciences of the United States of America* **2004**;101:8699-704
17. Silk AD, Zasadil LM, Holland AJ, Vitre B, Cleveland DW, Weaver BA. Chromosome missegregation rate predicts whether aneuploidy will promote or suppress tumors. *Proceedings of the National Academy of Sciences of the United States of America* **2013**;110:E4134-41
18. Andor N, Maley CC, Ji HP. Genomic Instability in Cancer: Teetering on the Limit of Tolerance. *Cancer research* **2017**;77:2179-85
19. Jemaa M, Galluzzi L, Kepp O, Senovilla L, Brands M, Boemer U, *et al.* Characterization of novel MPS1 inhibitors with preclinical anticancer activity. *Cell Death Differ* **2013**;20:1532-45
20. Liu Y, Lang Y, Patel NK, Ng G, Laufer R, Li SW, *et al.* The Discovery of Orally Bioavailable Tyrosine Threonine Kinase (TTK) Inhibitors: 3-(4-(heterocyclyl)phenyl)-1H-indazole-5-carboxamides as Anticancer Agents. *J Med Chem* **2015**;58:3366-92
21. Colombo R, Caldarelli M, Mennecozzi M, Giorgini ML, Sola F, Cappella P, *et al.* Targeting the mitotic checkpoint for cancer therapy with NMS-P715, an inhibitor of MPS1 kinase. *Cancer Res* **2010**;70:10255-64
22. Naud S, Westwood IM, Faisal A, Sheldrake P, Bavetsias V, Atrash B, *et al.* Structure-based design of orally bioavailable 1H-pyrrolo[3,2-c]pyridine inhibitors of mitotic kinase monopolar spindle 1 (MPS1). *J Med Chem* **2013**;56:10045-65
23. Faisal A, Mak GWY, Gurden MD, Xavier CPR, Anderhub SJ, Innocenti P, *et al.* Characterisation of CCT271850, a selective, oral and potent MPS1 inhibitor, used to

- directly measure in vivo MPS1 inhibition vs therapeutic efficacy. *British journal of cancer* **2017**;116:1166-76
24. Innocenti P, Woodward HL, Solanki S, Naud S, Westwood IM, Cronin N, *et al.* Rapid Discovery of Pyrido[3,4-d]pyrimidine Inhibitors of Monopolar Spindle Kinase 1 (MPS1) Using a Structure-Based Hybridization Approach. *Journal of medicinal chemistry* **2016**;59:3671-88
 25. Mason JM, Wei X, Fletcher GC, Kiarash R, Brokx R, Hodgson R, *et al.* Functional characterization of CFI-402257, a potent and selective Mps1/TTK kinase inhibitor, for the treatment of cancer. *Proceedings of the National Academy of Sciences of the United States of America* **2017**;114:3127-32
 26. Laufer R, Li SW, Liu Y, Ng G, Lang Y, Feher M, *et al.* Discovery of 4-(4-aminopyrazolo[1,5-a][1,3,5]triazin-8-yl)benzamides as novel, highly potent and selective, orally bioavailable inhibitors of Tyrosine Threonine Kinase, TTK. *Bioorganic & medicinal chemistry letters* **2016**;26:3562-6
 27. Perou CM, Sorlie T, Eisen MB, van de Rijn M, Jeffrey SS, Rees CA, *et al.* Molecular portraits of human breast tumours. *Nature* **2000**;406:747-52
 28. Sorlie T, Perou CM, Tibshirani R, Aas T, Geisler S, Johnsen H, *et al.* Gene expression patterns of breast carcinomas distinguish tumor subclasses with clinical implications. *Proceedings of the National Academy of Sciences of the United States of America* **2001**;98:10869-74
 29. Sorlie T, Wang Y, Xiao C, Johnsen H, Naume B, Samaha RR, *et al.* Distinct molecular mechanisms underlying clinically relevant subtypes of breast cancer: gene expression analyses across three different platforms. *BMC genomics* **2006**;7:127
 30. O'Brien KM, Cole SR, Tse CK, Perou CM, Carey LA, Foulkes WD, *et al.* Intrinsic breast tumor subtypes, race, and long-term survival in the Carolina Breast Cancer Study. *Clin Cancer Res* **2010**;16:6100-10
 31. Kim MJ, Ro JY, Ahn SH, Kim HH, Kim SB, Gong G. Clinicopathologic significance of the basal-like subtype of breast cancer: a comparison with hormone receptor and Her2/neu-overexpressing phenotypes. *Human pathology* **2006**;37:1217-26
 32. Sotiriou C, Neo SY, McShane LM, Korn EL, Long PM, Jazaeri A, *et al.* Breast cancer classification and prognosis based on gene expression profiles from a population-based study. *Proceedings of the National Academy of Sciences of the United States of America* **2003**;100:10393-8
 33. Nishimura R, Osako T, Okumura Y, Hayashi M, Toyozumi Y, Arima N. Ki-67 as a prognostic marker according to breast cancer subtype and a predictor of recurrence time in primary breast cancer. *Experimental and therapeutic medicine* **2010**;1:747-54
 34. Kolacinska A, Chalubinska J, Zawlik I, Szymanska B, Borowska-Garganisz E, Nowik M, *et al.* Apoptosis-, proliferation, immune function-, and drug resistance- related genes in ER positive, HER2 positive and triple negative breast cancer. *Neoplasma* **2012**;59:424-32
 35. Workman P, Aboagye EO, Balkwill F, Balmain A, Bruder G, Chaplin DJ, *et al.* Guidelines for the welfare and use of animals in cancer research. *British journal of cancer* **2010**;102:1555-77
 36. Woodward HLI, P. Cheung, K. J. Hayes, A. Roberts, J. Henley, A. T. Faisal, A. Mak, G. W. Box, G. Westwood, I. M. Cronin, N. Carter, M. Valenti, M. De Haven-Brandon, A. O'Fee, L. Saville, H. Schmitt, J. Burke, R. Broccatelli, F. van Montfort, R. L. M Raynaud, F. I. Eccles, S. A. Linardopoulos, S. Blagg, J. Hoelder, S. Introduction of a Methyl Group Curbs Metabolism of Pyrido[3,4- d]pyrimidine Monopolar Spindle 1 (MPS1) Inhibitors and Enables the Discovery of the Phase 1 Clinical Candidate N2-(2-

- Ethoxy-4-(4-methyl-4 H-1,2,4-triazol-3-yl)phenyl)-6-methyl- N8-neopentylpyrido[3,4-d]pyrimidine-2,8-diamine (BOS172722). *J Med Chem* **2018**;61:8226–40
37. Brough R, Frankum JR, Sims D, Mackay A, Mendes-Pereira AM, Bajrami I, *et al.* Functional viability profiles of breast cancer. *Cancer Discov* **2011**;1:260-73
 38. Wortzel I, Hanoch T, Porat Z, Hausser A, Seger R. Mitotic Golgi translocation of ERK1c is mediated by a PI4KIIIbeta-14-3-3gamma shuttling complex. *Journal of cell science* **2015**;128:4083-95
 39. Neumann B, Walter T, Heriche JK, Bulkescher J, Erfle H, Conrad C, *et al.* Phenotypic profiling of the human genome by time-lapse microscopy reveals cell division genes. *Nature* **2010**;464:721-7
 40. Brownlee PM, Meisenberg C, Downs JA. The SWI/SNF chromatin remodelling complex: Its role in maintaining genome stability and preventing tumourigenesis. *DNA repair* **2015**;32:127-33
 41. Haren L, Merdes A. Direct binding of NuMA to tubulin is mediated by a novel sequence motif in the tail domain that bundles and stabilizes microtubules. *Journal of cell science* **2002**;115:1815-24
 42. Yan K, Li L, Wang X, Hong R, Zhang Y, Yang H, *et al.* The deubiquitinating enzyme complex BRISC is required for proper mitotic spindle assembly in mammalian cells. *The Journal of cell biology* **2015**;210:209-24
 43. Lee SH, Sterling H, Burlingame A, McCormick F. Tpr directly binds to Mad1 and Mad2 and is important for the Mad1-Mad2-mediated mitotic spindle checkpoint. *Genes & development* **2008**;22:2926-31
 44. Patel N, Weekes D, Drosopoulos K, Gazinska P, Noel E, Rashid M, *et al.* Integrated genomics and functional validation identifies malignant cell specific dependencies in triple negative breast cancer. *Nature communications* **2018**;9:1044
 45. Prichard MN, Shipman C, Jr. A three-dimensional model to analyze drug-drug interactions. *Antiviral research* **1990**;14:181-205
 46. Zasadil LM, Andersen KA, Yeum D, Rocque GB, Wilke LG, Tevaarwerk AJ, *et al.* Cytotoxicity of paclitaxel in breast cancer is due to chromosome missegregation on multipolar spindles. *Sci Transl Med* **2014**;6:229ra43
 47. Yamagishi Y, Yang CH, Tanno Y, Watanabe Y. MPS1/Mph1 phosphorylates the kinetochore protein KNL1/Spc7 to recruit SAC components. *Nat Cell Biol* **2012**;14:746-52
 48. Xiao H, Verdier-Pinard P, Fernandez-Fuentes N, Burd B, Angeletti R, Fiser A, *et al.* Insights into the mechanism of microtubule stabilization by Taxol. *Proceedings of the National Academy of Sciences of the United States of America* **2006**;103:10166-73
 49. Janssen A, Kops GJ, Medema RH. Elevating the frequency of chromosome mis-segregation as a strategy to kill tumor cells. *Proc Natl Acad Sci U S A* **2009**;106:19108-13
 50. Hiruma Y, Sacristan C, Pachis ST, Adamopoulos A, Kuijt T, Ubbink M, *et al.* CELL DIVISION CYCLE. Competition between MPS1 and microtubules at kinetochores regulates spindle checkpoint signaling. *Science* **2015**;348:1264-7

Figures

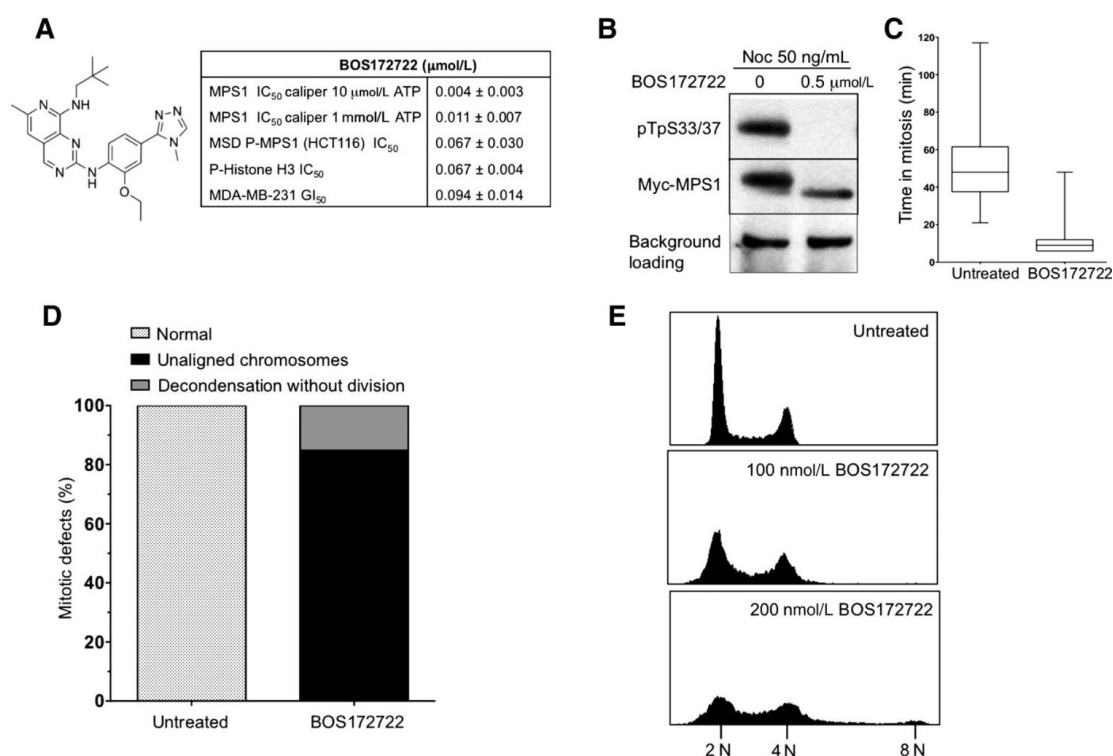


Figure 1. BOS172722 structure and characterization in biochemical and cellular assays. **A.** Structure and biochemical and cellular activity of BOS172722. **B.** Myc-MPS1-expressed nocodazole-arrested HCT116 cells treated with BOS172722 were tested for MPS1 inhibition. Background band was used as loading control. **C.** Box-and-whisker plot showing the time of HeLa cells in mitosis, in the absence or presence of BOS172722. The result was analyzed by Student's t-test ($p < 0.0001$). $N = 66$ cells per condition. **D.** Bar graph quantifying mitotic defects in HeLa cells treated with BOS172722. **E.** Flow cytometry cell-cycle profiles of HeLa cells treated with BOS172722.

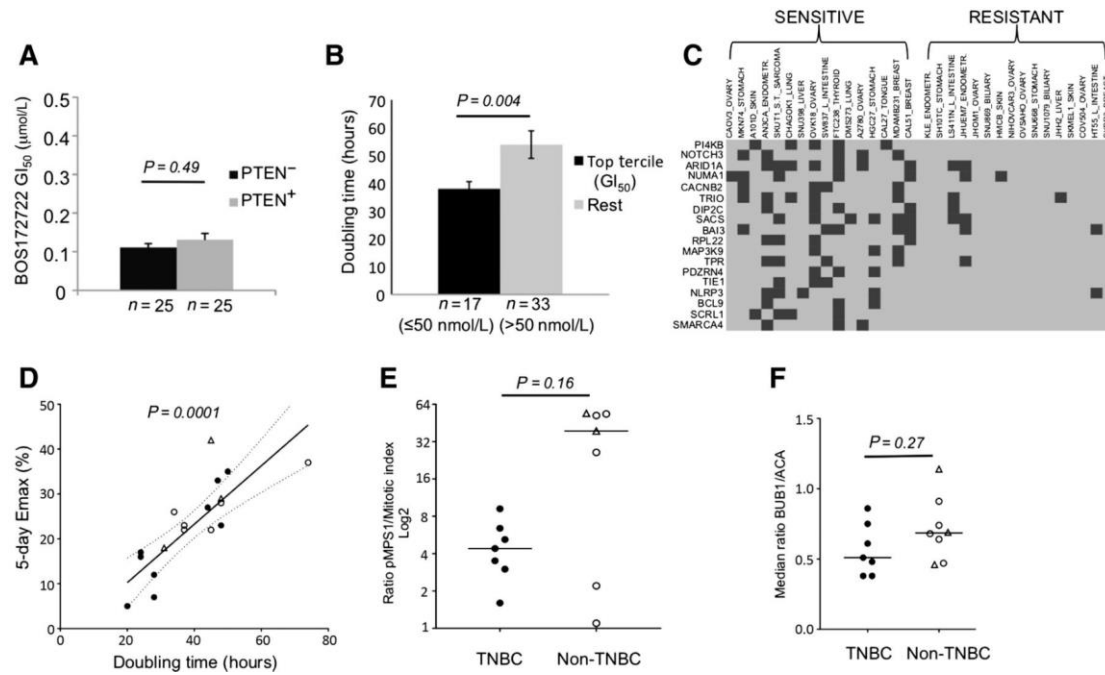


Figure 2. Association of BOS172722 *in vitro* potency with PTEN status, proliferation rate and SAC activity. **A.** Average GI_{50} of PTEN deficient (PTEN⁻) and PTEN proficient (PTEN⁺) cell lines. Bars represent standard error, p -value represents a two-tailed Student's t -test. **B.** Average doubling time for the top tercile of most sensitive cell lines *versus* the rest of the cell lines from the Horizon dataset. Bars represent standard error, p -value represents a two-tailed Student's t -test. **C.** Heatmap of mutated genes in cell lines with $GI_{50} < 50$ nM (SENSITIVE) and > 200 nM (RESISTANT). Dark squares are indicating the cell line with the corresponding mutated gene. **D.** Non-parametric Spearman correlation of E_{max} was measured by treatment of BOS172722 and doubling time in TNBC (black dots) and non-TNBC cell lines (white dots and triangles). White triangles in non-TNBC group indicate HER2 positive and overexpressed cell lines. The p -value is two-tailed and dot lines indicate 95% confidence interval of Spearman correlation. **E.** Scatter dot plot of the ratio of pT33pS37-MPS1 over mitotic index in TNBC and non-TNBC cell lines after Paclitaxel treatment. p -value represents a two-tailed Mann Whitney test. **F.** Scatter dot plot of the median ratio of BUB1 over ACA fluorescent signal in the kinetochore of TNBC and non-TNBC cell lines after Paclitaxel treatment. p -value represents a two-tailed Mann Whitney test.

Fi

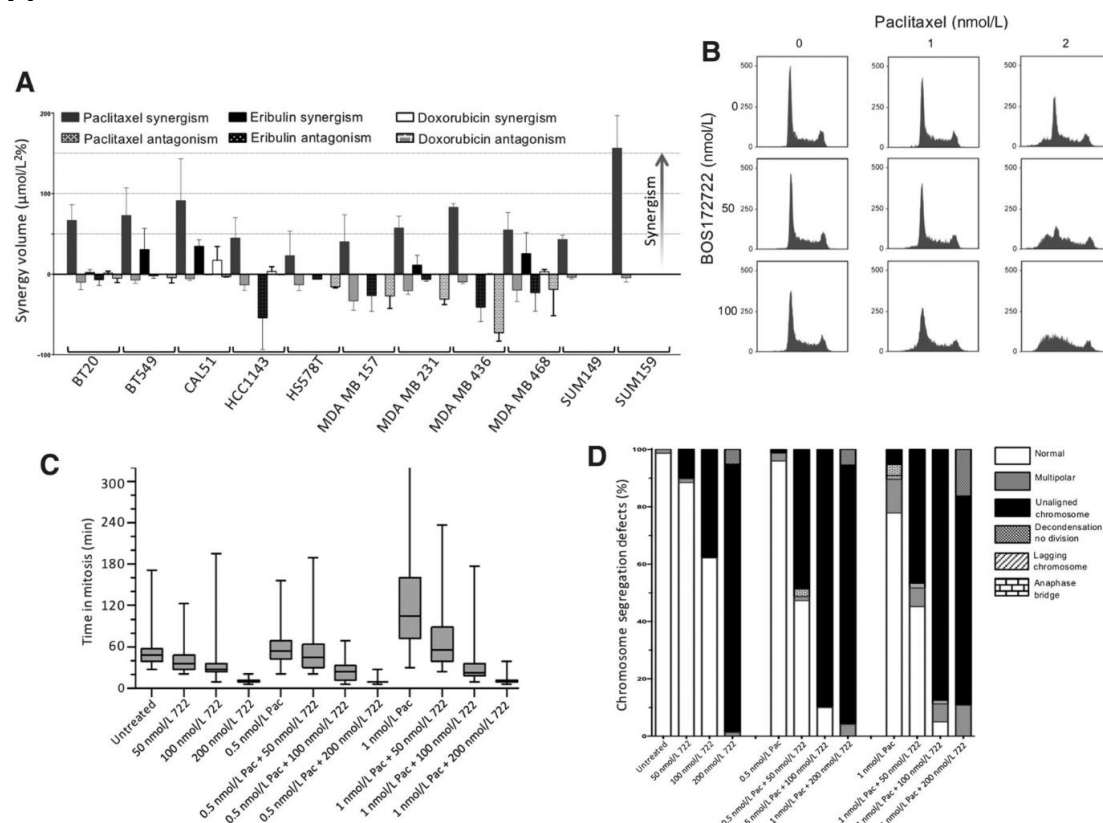


Figure 3. Synergy of BOS172722 with standard-of-care drugs in TNBC cell lines and mechanistic studies. **A.** Bar chart of synergism volumes of BOS172722 with Paclitaxel, Eribulin and Doxorubicin in TNBC cell lines. **B.** FACS analysis of the cell cycle distribution in MDA-MB-231 cells after 24h incubation with indicated drugs. **C.** Evaluation of the SAC in response to treatment with Paclitaxel and BOS172722. HeLa cells were incubated with Paclitaxel, BOS172722 or a combination of both. Mitotic timing was then assayed by live cell imaging as the time from nuclear envelope breakdown until the start of anaphase. Box plots show median, 25th to 75th percentile and min/max values. **D.** HeLa cells, stably transfected with H2B-mCherry, were treated with the indicated compounds. >60 cells were analysed for each condition. The graph depicts the quantification of chromosome alignment errors as measured by live cell imaging.

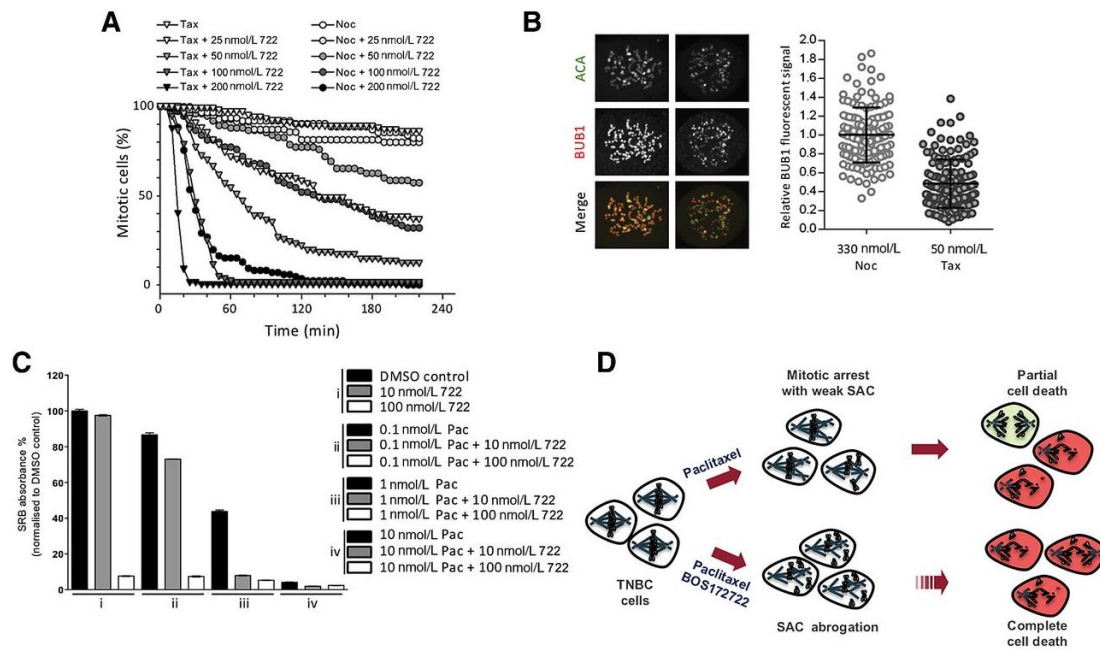


Figure 4. SAC response to microtubule stabilising and destabilising drugs. **A.** Comparison of SAC override by BOS172722 between Paclitaxel and nocodazole treated Hela cells. Plotted is the fraction of cells in mitosis at any given time. Only cells already arrested at the start of time-lapse imaging are included in the analysis with BOS172722 added to the cells at 0 minute. **B.** Quantification of BUB1 accumulation at centromeres in nocodazole and Paclitaxel-treated cells. Measurements were done in triplicate. **C.** Long-term proliferation assay. MDA-MB-231 cells were incubated with BOS172722, Paclitaxel and the combination of both for 24h. Whole cell growth was determined by SRB after 14 days. **D.** Model of the mechanism of synergism between BOS172722 and Paclitaxel.

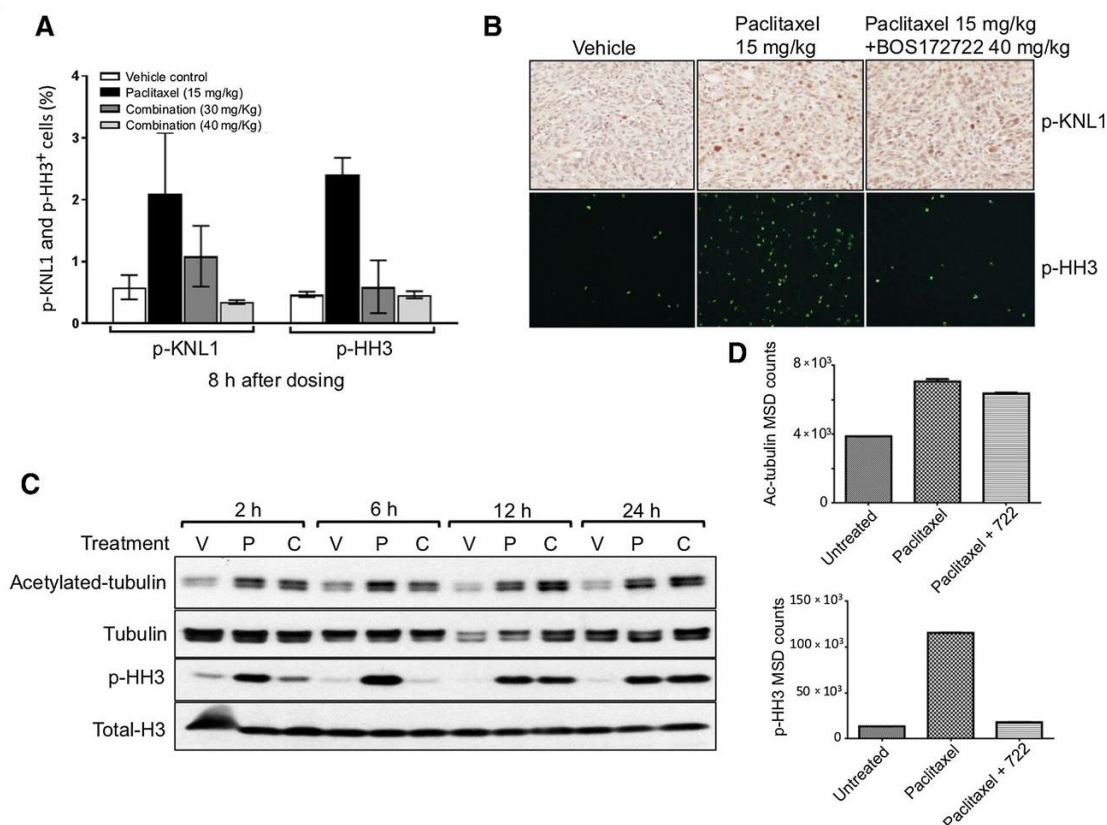


Figure 5. *In vivo* Pharmacodynamic studies of BOS172722. **A**, Pharmacodynamic analyses of Paclitaxel and BOS172722 in MDA-MB-231 subcutaneous human tumour xenografts. Vehicle, Paclitaxel alone and the simultaneous combination of Paclitaxel + BOS172722. Percentage of phospho-Histone H3 (p-HH3) positive cells by immunofluorescence and p-KNL1 by immunohistochemistry staining at 8h after treatment. **B**. Representative images of staining at 8h after treatment. **C**. Immunoblot analysis of tumour lysates from HCT116 xenografts in athymic mice treated with vehicle (V), Paclitaxel alone (P) or Paclitaxel in combination with BOS172722 (C). Antibodies against acetylated and total tubulin, phosphorylated and total histone H3 were used at the indicated time points. **D**. MSD assays to measure the level of acetylated tubulin and phosphorylated Histone H3 in HCT116 xenografts.

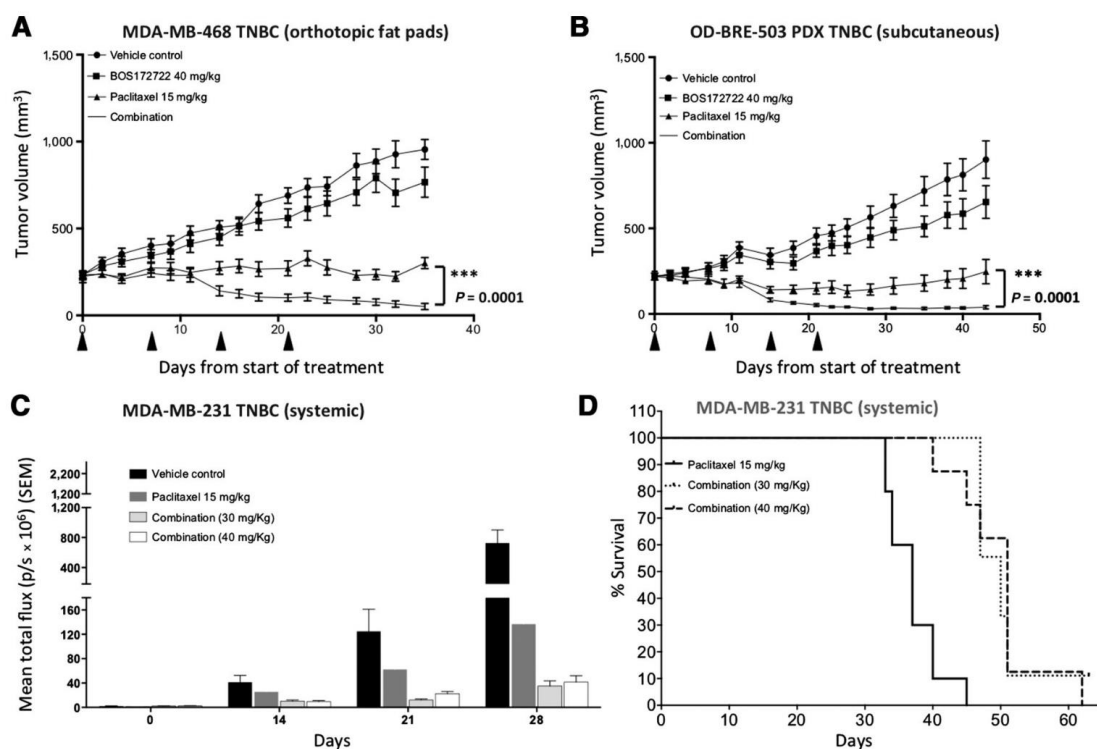


Figure 6. *In vivo* therapeutic activity of BOS172722 in TNBC models. A. Tumour volumes were plotted-out to day 35 from the start of treatment when all cohorts were >80% complete. Arrows represent Paclitaxel treatment days; ***: 2-way RM ANOVA $p < 0.0001$. **B.** Tumour volumes were plotted out to day 43 from the start of treatment when all cohorts were >80% complete. Arrows represent Paclitaxel treatment days; ***: 2-way RM ANOVA $p < 0.0001$. **C.** Metastasis model of MDA-MB-231 luciferase-expressing tumours in NOD SCID mice. On day 28, the flux in the treated groups (mean total flux \pm SEM) is indicated. **D,** Survival curves until day 63.